Magn Reson Med Sci 2018; 17; 251–258
doi:10.2463/mrms.mp.2017-0079
Published Online: December 5, 2017

MAJOR PAPER

Comparison of Glass Capillary Plates and Polyethylene Fiber Bundles as Phantoms to Assess the Quality of Diffusion Tensor Imaging

Atsushi Tachibana[1,2], Yasuhiko Tachibana[2*], Jeff Kershaw[2], Hiromi Sano[2], Masahiro Fukushi[1], and Takayuki Obata[2]

Purpose: The purpose of this study was to evaluate the suitability of two phantoms, one made of capillary plates and the other polyethylene fibers, for assessing the quality of diffusion tensor imaging (DTI).

Methods: The first phantom was a stack of glass capillary plates with many parallel micropores (CP). The second phantom was a bundle of polyethylene fiber Dyneema held together with a thermal shrinkage tube (Dy). High resolution multi-shot echo planar imaging (EPI) DTI acquisitions were performed at b-values of 0 and 1000 s/mm^2 and diffusion-times (T_{diff}) of 37.7 and 97.7 ms on a preclinical 7T MRI scanner. Thirty diffusion-encoding directions were used. The data were used to calculate the fractional anisotropy (FA), mean diffusivity (MD), and angular dispersion (AD). Further acquisitions were performed at b-values from 0 to 8000 s/mm^2 in 14 steps with the diffusion gradient applied parallel (axial) and perpendicular (radial) to the Z direction. On the other hand, the data acquired with a 3T MRI scanner were used to confirm that measurements on a clinical machine are consistent with the 7T MRI results.

Results: The dependence of FA, MD and AD on T_{diff} was smaller for the Dy than for the CPs. The b-value-dependent signal attenuations in the axial direction at T_{diff} = 37.7 and 97.7 ms were similar for both phantoms. In the radial direction, Dy demonstrated similar b-value attenuation to that of *in vivo* tissue for both T_{diff}s, but the attenuation for the CPs was affected by the change in T_{diff}. Parameter estimates were similar for 3T and 7T MRI.

Conclusion: The characteristics of the CP indicate that it can be used as a restricted-diffusion dominant phantom, while the characteristics of the Dy suggest that it can be used as a hindered-diffusion dominant phantom. Dy may be more suitable than CP for DTI quality control.

Keywords: *diffusion tensor imaging, diffusion-time, high b-value, magnetic resonance imaging, phantom*

Introduction

Diffusion tensor imaging (DTI) facilitates the quantitative measurement of anisotropy and orientation characteristics of water diffusivity.[1] In clinical diagnostic imaging, the DTI technique is known to have a high degree of usability for brain white matter that is rich in nerve fibers.[2,3] The calculable DTI estimates such as fractional anisotropy (FA) and mean diffusivity (MD) are commonly used as quantitative parameters that reflect the density and direction of nerve fibers.[4] On the other hand, the parameters for imaging should be optimized separately for each MRI scanner in terms of gradient strength, magnetic field and adopted pulse sequence, as they differ for different MRI scanners and/or different facilities and greatly influence the image quality and contrast of DTI. Therefore, quality control (QC) using a standard phantom is necessary to maintain uniformity of the image quality and contrast.[5] This is especially important in cases where the images from multiple facilities or scanners need to be handled equally without considering such differences (e.g. multi-center study).[6,7] QC itself is widely performed in daily clinics, but standard water phantoms for such general checks are not optimal for DTI validation because they do not contain diffusional anisotropy. Therefore, special DTI-QC phantoms that have an appropriate diffusional anisotropy are needed. It should be noted that the main target of DTI is brain white matter, so the diffusional properties of the DTI-QC phantom should be similar to those of brain white matter.[8]

[1]Department of Radiological Sciences, Graduate School of Human Health Sciences, Tokyo Metropolitan University, Tokyo, Japan
[2]Applied MRI Research, Department of Molecular Imaging and Theranostics, National Institute of Radiological Sciences, National Institutes for Quantum and Radiological Science and Technology, 4-9-1 Anagawa, Inage-ku, Chiba, Chiba 263-8555, Japan
*Corresponding author, Phone: +81-43-206-3230, Fax: +81-43-251-4534, E-mail: yaz.tachibana@radio.email.ne.jp

Received: May 28, 2017 | Accepted: September 14, 2017

Biological phantoms such as fibrous vegetables and animal nerve tissues are generally used as DTI phantoms. The advantages of these phantoms are, first, that they have high diffusional anisotropy, and second, the expected range of the diffusion estimates FA and MD are close to those of *in vivo* tissues.[9–11] However, they are not suitable as standard QC phantoms because they do not have high reproducibility, stability, and the period of time that the phantom can be kept without denaturation is limited. To overcome these problems, non-biological phantoms made of materials such as glass plates or chemical fibers are proposed. Capillary phantoms made of glass or plastic plates with many micropores oriented in parallel are known to have high diffusional anisotropy, high reproducibility and stability, but they are limited in the types of *in vivo* architectural structure they can simulate.[5,12,13] On the other hand, synthetic fibers (especially Dyneema), due to their flexibility, can be freely oriented to create a phantom. In addition, the range of FA and MD measured in fiber-phantoms is relatively close to brain white matter, so they are useful as DTI phantoms.[14–16] In any case, the detailed diffusional characteristics of both fiber-phantoms and capillary phantoms have as yet not been evaluated sufficiently. This is because of recent advances in both preclinical and clinical scanner capability. Higher b-values over a wide range are now often used for diffusion-encoding, but the diffusional characteristics of the phantoms at these high b-values have not yet been well confirmed. Also, the influence of different diffusion-times on the diffusion estimates of the phantoms is unknown. In spite of the importance of diffusion-time in measuring diffusion, the relevant parameters in commercial clinical scanners are usually automatically determined according to the desired b-value and device-specific performance. In addition, as the applied parameters are usually not displayed on clinical scanners, even checking the exact diffusion-time of each scan is difficult. Therefore, low diffusion-time dependence of the measured estimates is a desirable feature for a standard DTI phantom. Moreover, diffusion in white matter, which is the main target of DTI, is generally regarded as less dependent on diffusion-time in usual clinical settings.[17]

By performing DTI at multiple b-values and diffusion-times, the purpose of this study is to evaluate the usefulness of phantoms made of capillary plates or polyethylene fibers as potential QC phantoms.

Materials and Methods

In this study, we first created a DTI phantom made of glass capillary plates and Dyneema fibers as described in detail in the following sections. We then assessed their applicability as a standard DTI phantom using 7T and 3T MRI systems. The detailed diffusional characteristics of the phantoms were evaluated mainly using the data acquired with 7T MRI. Common DTI estimates, including FA and MD, that can be calculated by fitting the multiple diffusion-time and multiple b-value signal intensities to a bi-exponential curve were assessed for this purpose. On the other hand, the 3T MRI data were used mainly to confirm whether the results found from the 7T MRI data were reproducible on clinical machines.

Phantoms

The following materials were used to create the DTI phantoms. The first phantom was a capillary plate phantom (CP) that used several capillary plates (Hamamatsu Photonics K.K., Shizuoka, Japan) as its main structure. A capillary plate is made of glass material and has many parallel micro-capillaries (20-μm diameter) arranged uniformly (Fig. 1a). The plates were stacked in a plastic tube (10-mm diameter) and were sealed after filling with ultra-pure water. The second phantom was a Dyneema phantom (Dy; TOYOBO CO., LTD., Osaka, Japan), made with hydrophobic polyethylene fibers (Fig. 1b). To create Dy, 160 Dyneema fibers were bundled in a heat-shrinkable tube and placed in heated water (95°C). This step was completely performed under-water with ultra-pure water to avoid air contamination. Further, with the bundle of fibers still submerged in ultra-pure water, the container was placed in a vacuum pump and degassed for 20 minutes to remove micro-air bubbles. Finally, while still under-water the bundle was sealed in a plastic tube (10-mm diameter) with ultra-pure water.

DTI scanning

A preclinical 7T MRI system (Magnet; Japan Superconductor Technology, Inc. and Kobe Steel, Ltd., Hyogo, Japan: Console; Bruker BioSpin Corporation, Billerica, MA, USA) equipped with a small rodent brain surface coil (Rapid Biomedical) for reception and a 12-cm inner diameter volume coil for transmission (Rapid Biomedical) was used for the main acquisitions of this study. The phantoms were placed parallel with the Z axis direction of the MRI gantry, and then DTI scans at 14 different b-values (0, 2, 250, 500, 750, 1000, 1500, 2000, 3000, 4000, 5000, 6000, 7000 and 8000 s/mm^2) with 30 different diffusion-encoding directions were obtained for two different diffusion-time lengths (T_{diff}) = $\Delta - \delta/3$, 37.7 and 97.7 ms. The duration of the motion probing gradients (MPG) (δ) was fixed at 7 ms, and the time between the onsets of the MPG lobes (Δ) was 40 and 100 ms for the shorter and longer T_{diff}s, respectively. Acquisition was performed with high resolution multi-shot echo planar imaging (EPI). The other major scanning parameters were: TR = 3000 ms, TE = 115 ms, average = 1, EPI factor = 4, FOV = 25.6 × 25.6 mm, matrix size = 128 × 128, resolution = 0.2 × 0.2 × 2.0 mm, temperature of magnet room approximately 22°C, total scan time = 78 min.

An additional DTI scan representing a typical clinical acquisition was obtained with a 3T MRI system (MAGNETOM Verio 3T; Siemens Healthcare K.K., Erlangen, Germany) equipped with a 12-channel head coil. The phantoms were placed parallel with the Z axis direction of the MRI gantry, and then the DTI scan was done using b-values of 0 and

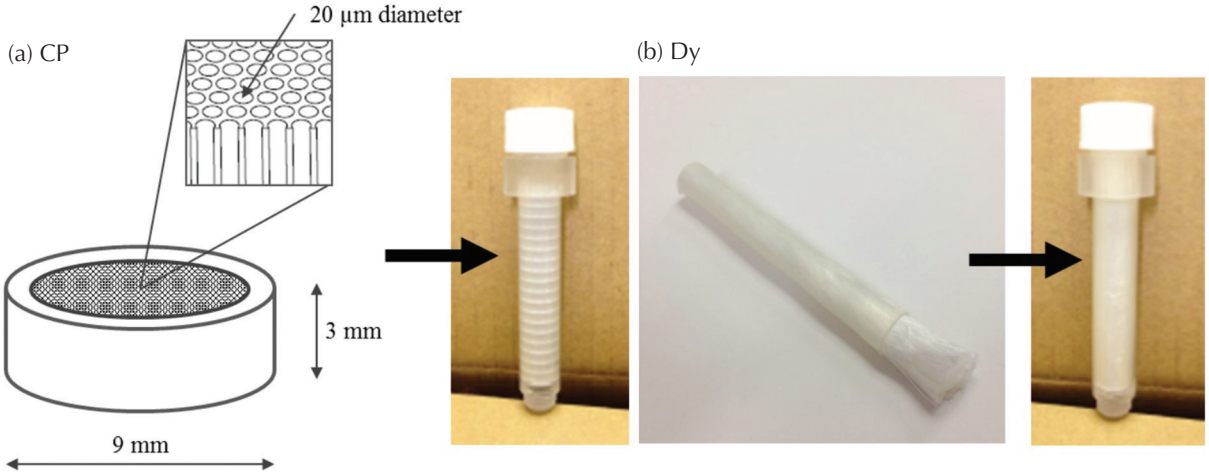

Fig. 1 Capillary plate phantom (CP) and Dyneema phantom (Dy). (**a**) A capillary plate is made of glass, and has many micropores (20 μm diameter) that are uniformly spaced in parallel. To create the CP, several plates were stacked in a plastic tube with ultra-pure water. (**b**) A bundle of polyethylene fibers (Dyneema, TOYOBO CO., LTD., Osaka, Japan) were bunched together with a thermal shrinkage tube to create the Dy.

1000 s/mm^2 in 12 different diffusion-encoding directions. Segmented multi-shot EPI (RESOLVE) acquisition was applied to minimize artifacts.[18] Of note, T_{diff} was automatically selected by the MRI system for this additional scan, but it was not displayed on the user interface as is usual for clinical machines. The other major parameters were: TR = 5000 ms, TE = 72 ms, average = 2, number of b = 0 images = 1, number of readout segments = 5, FOV = 200.0 × 200.0 mm, matrix size = 100 × 100, resolution = 2.0 × 2.0 × 2.0 mm, temperature of magnet room approximately 22°C, total scan time = 13 min.

Finally, to investigate the long-term stability of phantom DTI estimates, the 3T MRI was repeated on the same phantom at 150 days after the original (day 0) experiments. In addition, the reproducibility of the manufacturing process for the Dy was tested by performing 3T MRI on four additional phantoms made in the same way as described above. Analysis of the data was performed in the same way as for the other data.

Analysis of basic DTI parameters

In this section, we used the 7T and 3T scanner data separately to calculate the estimates described below. The slice with the largest cross-sectional area of the phantoms on the FA maps was selected, and then a ROI was manually drawn on the image to extract data for analysis. The same ROI was used for all further analysis. The detailed position of the ROIs is shown on the 7T (T_{diff} = 37.7 and 97.7 ms) and 3T MRI FA maps in Fig. 2.

First, as the most common DTI estimates, FA and MD were calculated pixel-by-pixel from the b = 0 and 1000 s/mm^2 data. The mean value of the pixels inside the ROI was used for analysis. Second, to quantitatively assess the homogeneity of diffusional anisotropy, an index named AD_{50} was defined and calculated for this study as follows. As the first step, the mean principal eigenvector (MPEV) inside the ROI was determined as

$$MPEV = \frac{\sum_{i=1}^{n}(\boldsymbol{v}_{1i})}{\left|\sum_{i=1}^{n}(\boldsymbol{v}_{1i})\right|} \quad (1),$$

where $\boldsymbol{v}_{1i}$ indicates the first eigenvector for each pixel i, and n is the number of pixels inside the ROI. Then, the angular dispersion (AD) between MPEV and the first eigenvector of each pixel, AD_i, was defined as

$$\cos(AD_i) = \frac{|\boldsymbol{v}_{1i} \cdot MPEV|}{|\boldsymbol{v}_{1i}| \cdot |MPEV|} \quad (2).$$

The AD_i ranges from 0 to 90 degrees and a smaller value of AD_i indicates closer alignment with the mean direction of diffusional anisotropy, i.e. the MPEV. Finally, AD_{50} was defined as the median of the AD_i values inside the ROI. Thus, AD_{50} was an index reflecting the variation of the major diffusing directions inside the ROI.

The estimates calculated above (i.e. FA, MD, AD_{50}) were compared between CP and Dy, and also for different T_{diff}s.

Analysis for diffusion-time dependency in multiple b-value DTI

The analysis of this section was done using the data of 7T MRI. First, the multiple b-value and multiple-T_{diff} images acquired with the diffusion-encoding direction parallel or perpendicular to the Z axis were selected as axial and radial diffusion-weighted imagings (DWIs), respectively. The ROI drawn in the previous section was then applied to these images to extract the pixelwise axial and radial b-value-related signal changes at different T_{diff}s. The

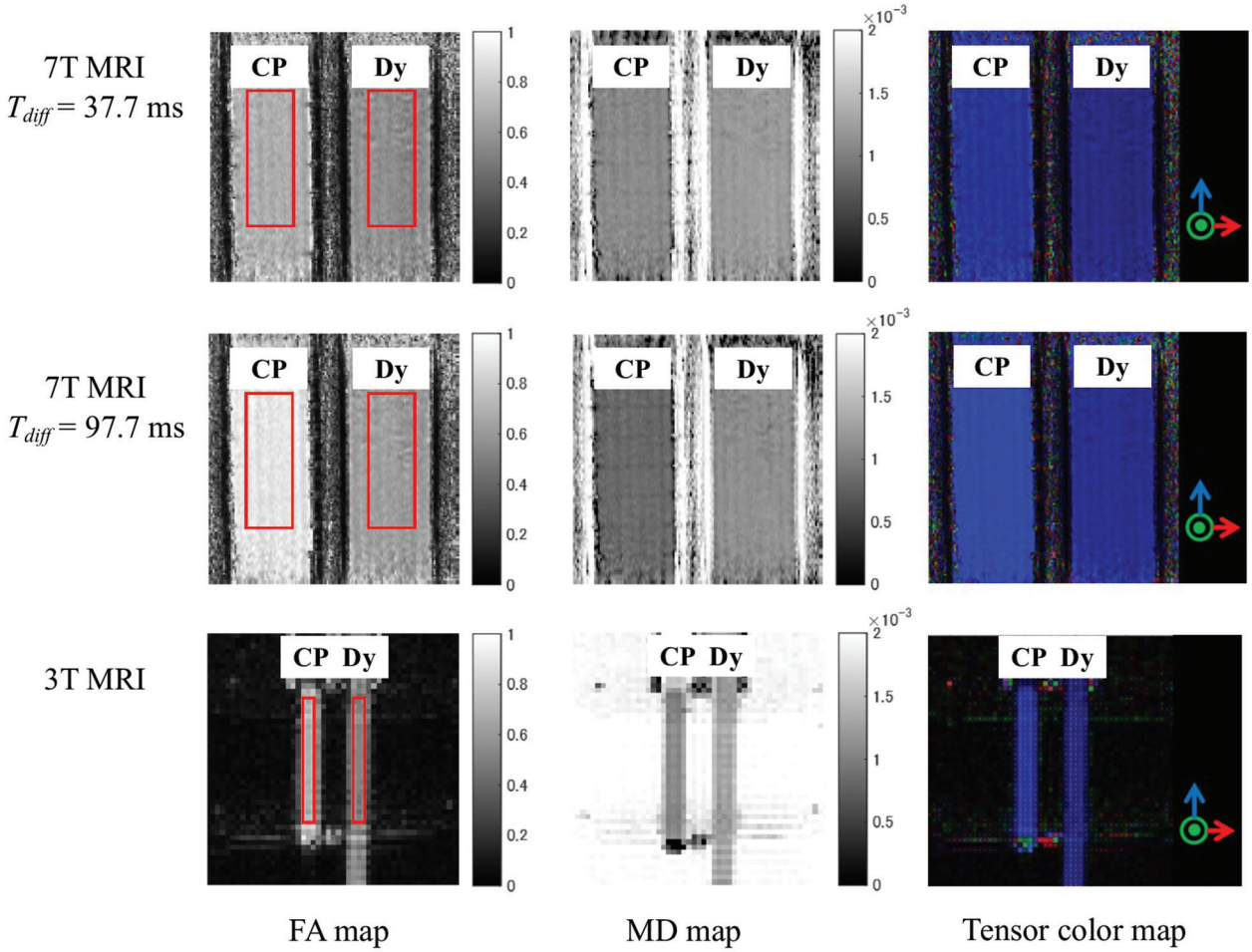

Fig. 2 Fractional anisotropy (FA), mean diffusivity (MD), and diffusion tensor maps. The maps were obtained from both preclinical 7T and clinical 3T MRI. In the diffusion tensor color maps, diffusivity in the *x*, *y*, and *z* directions is coded as red, green, and blue, respectively. The maps demonstrate the highly homogeneous diffusion properties of both the CP and Dy. The results differed for different T_{diff}s, but visual homogeneity was consistent. The red rectangle drawn on the FA maps indicates the ROIs selected for further analysis. CP, Capillary plate phantom; Dy, Dyneema phantom; T_{diff}, diffusion-time.

multiple b-value signal was fitted to a bi-exponential curve for each T_{diff} using,

$$\frac{S(b)}{S_0} = (f_{fast}) \cdot \exp(-bD_{fast}) + (1 - f_{fast}) \cdot \exp(-bD_{slow}) \quad (3),$$

where $S(b)/S_0$ was the normalized signal intensity, b was the b-value, D_{fast} and D_{slow} were the diffusion coefficients of the fast and slow diffusion compartments, and f_{fast} was the volume fraction of the fast diffusion compartment. The estimates of D_{fast}, D_{slow}, and f_{fast} were averaged inside the ROI. These averaged estimates were compared between CP and Dy in terms of their dependency on T_{diff}.

Results

Analysis of basic DTI estimates

From visual inspection, the FA, MD and tensor color maps of the phantoms all showed high homogeneity for both 7T and 3T MRI (Fig. 2). This is further demonstrated by the relatively small standard deviation of the DTI estimates in the ROIs (Tables 1 and 2).

Details of the calculated estimates (FA, MD, AD_{50}) are shown in Tables 1 and 2 for the 7T and 3T data, respectively. At 7T, the mean MD and FA of Dy at T_{diff} = 37.7 ms were 1.2 × 10^{-3} mm^2/s and 0.55, respectively, and those of T_{diff} = 97.7 ms were 1.1 × 10^{-3} mm^2/s and 0.61, respectively (Table 1). For CP at 7T, the mean MD and FA at T_{diff} = 37.7 ms were 1.1 × 10^{-3} mm^2/s and 0.68, respectively, and those at T_{diff} = 97.7 ms were 0.83 × 10^{-3} mm^2/s and 0.89, respectively (Table 1). To summarize, mean MD decreased and mean FA increased for both CP and Dy when T_{diff} increased from 37.7 to 97.7 ms.

At 3T, at day 0 the mean MD and FA for Dy were 1.3 × 10^{-3} mm^2/s and 0.53, respectively, while the same values for CP were 1.1 × 10^{-3} mm^2/s and 0.72, respectively (Table 2). Identical measurements 150 days later found similar values for mean MD and FA, which suggests long-term stability of measurements on both phantoms.

Table 1. Diffusion estimates obtained for the CP and Dy using preclinical 7T MRI

	T_{diff} = 37.7 ms		T_{diff} = 97.7 ms	
	CP	Dy	CP	Dy
FA	0.68 ± 0.030	0.55 ± 0.040	0.89 ± 0.030	0.61 ± 0.030
MD ($\times 10^{-3}$ mm^2/s)	1.1 ± 0.040	1.2 ± 0.050	0.83 ± 0.040	1.1 ± 0.050
AD_{50} (degrees)	2.2	2.9	1.7	2.4

Numbers indicate mean and standard deviation of the estimates. AD_{50}, a measure of uniformity of diffusion anisotropy defined in this study (see main body); CP, Capillary Plate phantom; Dy, Dyneema phantom; T_{diff}, diffusion time; FA, Fractional Anisotropy; MD, Mean Diffusivity.

Table 2. Diffusion estimates obtained for the CP and Dy at day 0 and 150 using 3T MRI

	CP		Dy	
	Day 0	Day 150	Day 0	Day 150
FA	0.72 ± 0.035	0.70 ± 0.028	0.53 ± 0.042	0.53 ± 0.035
MD ($\times 10^{-3}$ mm^2/s)	1.1 ± 0.055	1.0 ± 0.081	1.3 ± 0.070	1.2 ± 0.038
AD_{50} (degrees)	1.9	2.2	2.1	3.5

Numbers indicate mean and standard deviation of the estimates. AD_{50}, a measure of uniformity of diffusion anisotropy defined in this study (see main body); CP, Capillary Plate phantom; Dy, Dyneema phantom; FA, Fractional Anisotropy; MD, Mean Diffusivity.

Table 3. Diffusion estimates obtained from four different Dys using 3T MRI

	Dy #1	Dy #2	Dy #3	Dy #4
FA	0.52 ± 0.048	0.53 ± 0.030	0.53 ± 0.025	0.52 ± 0.029
MD ($\times 10^{-3}$ mm^2/s)	1.2 ± 0.056	1.2 ± 0.037	1.2 ± 0.027	1.2 ± 0.041
AD_{50} (degrees)	3.9	2.8	2.6	2.7

Numbers indicate mean and standard deviation of the estimates. AD_{50}, a measure of uniformity of diffusion anisotropy defined in this study (see main body); Dy, Dyneema phantom; FA, Fractional Anisotropy; MD, Mean Diffusivity.

The estimates of AD_{50} were consistently larger for Dy (2.1–3.5) than for CP (1.7–2.2) for all cases (Tables 1 and 2). This difference may reflect the fact that the CP consists of a highly regular array of parallel pores, whereas it is expected that the fibers of the Dy have small random deviations away from a regular structure. Nevertheless, as AD_{50} may have values between 0 and 90 degrees, the difference between CP and Dy observed here is relatively small.

In comparison to the day 0 results for the Dy in Table 2, the measurements on the extra four Dy phantoms (Table 3) were very similar. These results indicate that the manufacturing process for Dy phantoms is highly reliable.

Analysis of diffusion-time-dependency in multiple b-value DTI

The b-value-dependent signal changes on the axial DWI were similar for both CP and Dy indicating that there was little dependence on T_{diff}s (Fig. 3). For both phantoms, the volume fraction of the fast diffusion compartment (f_{fast}) was close to 1, and the corresponding diffusion coefficient (D_{fast}) was close to 2.0×10^{-3} mm^2/s (Table 4).

On the other hand, CP and Dy had different signal-change patterns on the radial DWI. The difference in signal-change between different T_{diff}s was small for Dy, like those in the axial direction, but the difference was large for CP. The shape of the CP curve at T_{diff} = 97.7 ms meant that the results of bi-exponential curve fitting was poor (Fig. 3). Otherwise, f_{fast} for CP at T_{diff} = 37.7 ms was close to 1 (0.99), while for Dy it was 0.78 for both T_{diff}s. D_{fast} and D_{slow} for Dy at T_{diff} = 37.7 ms were 1.1 and 0.10×10^{-3} mm^2/s, respectively, and those at T_{diff} = 97.7 ms were 0.91 and 0.084×10^{-3} mm^2/s, respectively (Table 4).

Discussion

The results from analysis of the basic DTI parameters suggest that Dy may be more suitable as a standard DTI QC phantom. First, the homogeneity of the FA, MD and tensor color maps was similar for the CP and Dy. Also even though the value of AD_{50} was slightly larger for Dy than for CP, the range of values (2.1 – 3.5 vs. 1.7 – 2.2) indicate that the dispersion of the principal eigenvector across the ROI is quite small, which supports the homogeneity of both CP and Dy. Second, Dy may have diffusion estimates in a range favorable for a DTI QC phantom. The estimates obtained for the FA (0.53 – 0.61) and MD ($1.1 – 1.3 \times 10^{-3}$ mm^2/s) are comparable to those of white matter in human brain (FA = 0.60, MD = 1.2×10^{-3} mm^2/s).[17] The diffusion-time dependency of the Dy estimates

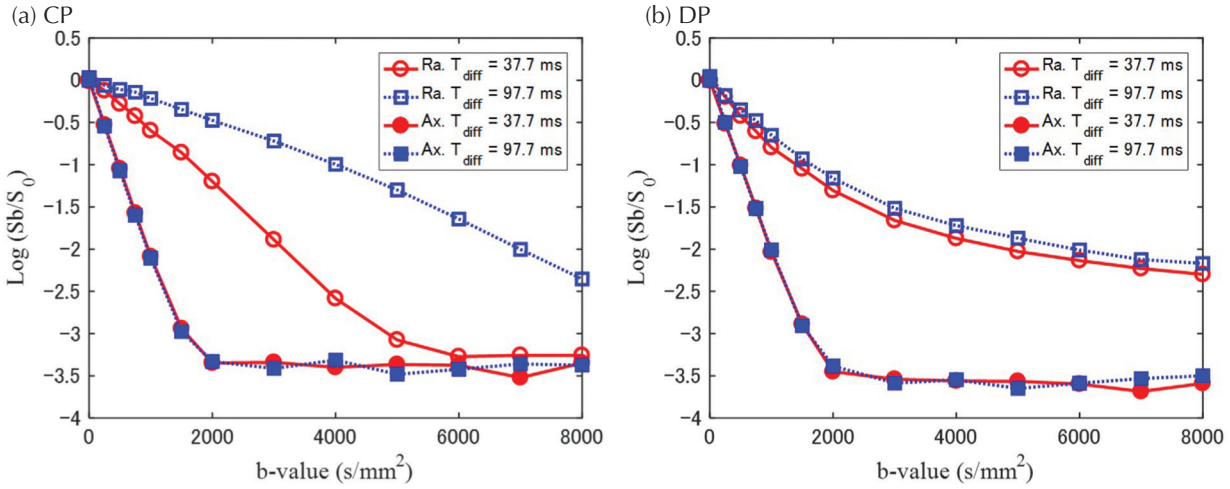

Fig 3. The b-value-dependent signal attenuations of the CP and Dy using preclinical 7T MRI. The graphs indicate the b-value-related signal change patterns of (**a**) CP and (**b**) Dy at T_{diff} = 37.7 ms and 97.7 ms. Signal changes in the axial direction were similar between the CP and Dy, and they were less dependent on T_{diff}. For the Dy, signal changes in the radial direction were similar at T_{diff} = 37.7 ms and 97.7 ms, while they were different for the CP at different T_{diff}s. In particular, the shape of the curve at T_{diff} = 97.7 ms for the CP meant that bi-exponential fitting was poor. CP, Capillary plate phantom; Dy, Dyneema phantom; T_{diff}, diffusion-time; Ra., radial diffusion-weighted imaging; Ax., axial diffusion-weighted imaging.

Table 4. Diffusion estimates obtained by fitting multiple b-value signals to a bi-exponential curve

	T_{diff} = 37.7 ms		T_{diff} = 97.7 ms	
	CP	Dy	CP	Dy
Axial				
f_{fast}	0.99	1.0	0.99	1.0
D_{fast} ($\times 10^{-3}$ mm^2/s)	2.1	2.1	2.0	2.0
D_{slow} ($\times 10^{-3}$ mm^2/s)	0.00	0.00	0.00	0.00
Radial				
f_{fast}	0.99	0.78	N/A (*)	0.78
D_{fast} ($\times 10^{-3}$ mm^2/s)	0.60	1.1	N/A (*)	0.91
D_{slow} ($\times 10^{-3}$ mm^2/s)	0.00	0.10	N/A (*)	0.084

Diffusion coefficients (D_{fast} and D_{slow}) and the fraction of fast diffusion compartment (f_{fast}) were obtained by fitting the multiple b-value diffusion weighted images to a bi-exponential curve. CP, Capillary Plate phantom; Dy, Dyneema phantom; T_{diff}, diffusion time; (*) The signals for the CP at T_{diff} = 97.7 ms were unable to be fitted.

was less than those for CP (Table 1). As mentioned in the introduction, since low dependence on diffusion-time is important for a reliable clinical standard phantom, Dy seems more advantageous than CP in this respect. Moreover, since this feature is common to both static magnetic field strengths used in this study, Dy may potentially have broad utility to be applied to various machines. The long-term stability and high reproducibility of the manufacturing process for Dy (Tables 2 and 3), further supports this.

With respect to the multiple b-value DTI (Fig. 3), the most prominent difference between the two phantoms was the diffusion-time dependency in the radial direction. The signal change pattern for Dy was similar for T_{diff} = 37.7 ms and T_{diff} = 97.7 ms, but the signal decay for CP was quite different between the two T_{diff}s, suggesting low and high dependence on diffusion-time, respectively. For brain white matter, it is usually empirically found that DWI signal attenuation with respect to b-value is fitted well by a bi-exponential equation (Eq. 3).[1] This was found to be true for the Dy signal change at both T_{diff}s, whereas for the CP the curve at T_{diff} = 97.7 ms was quantitatively different and bi-exponential fitting of the data was poor. In addition, the fitted estimates obtained for Dy at both T_{diff}s (Table 4) were consistent with those reported for brain white matter (f_{fast} = 0.80, D_{fast} = 0.82 $\times$ 10^{-3} mm^2/s, D_{slow} = 0.17 $\times$ 10^{-3} mm^2/s),[19] but those for CP at T_{diff} = 37.7 ms were not. Considering both the smaller dependency on diffusion-time and the fitted estimates closer to brain white matter, this further supports the view that Dy has an advantage as a standard DTI QC phantom compared to CP.

The difference in the b-value-dependent signal changes between CP and Dy in the radial direction is caused by the structural differences between the two phantoms. As Dy is made of a bundle of hydrophobic polyethylene fibers, when water molecules diffuse between these fibers in the radial direction, their motion is not free, but hindered.[20] Hindered diffusion is thought to be the major diffusion mode in brain white matter, and it is also less sensitive to diffusion-time for the range of values used in this study.[21] The results for Dy were consistent with this as they were far less dependent on T_{diff} than those for CP. On the other hand, as CP is composed of impermeable glass capillaries, the distance that water molecules can diffuse inside them in the radial direction (i.e. perpendicular to axial) is restricted. This is confirmed by the fact that the fitting results for CP were strongly influenced by T_{diff} (Fig. 3 and Table 4). From this point of view, diffusion in the CP is not suitable for a DTI phantom for *in vivo* MRI.

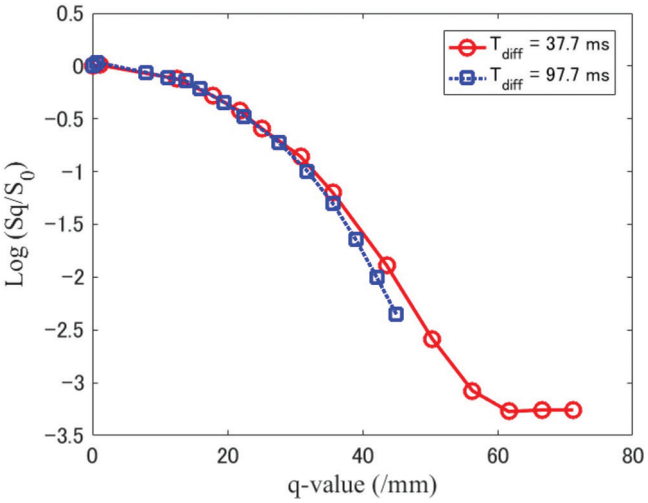

Fig. 4 Preclinical 7T MRI signal changes plotted as a function of q-value for the CP in radial direction. The q-value-related signal changes at T_{diff} = 37.7 and 97.7 ms are similar when plotted as a function of q. This indicates that the majority of the difference between the radial signal decay curves when plotted against b-value (Fig. 3), is due to the different T_{diff}s. CP, Capillary plate phantom; T_{diff}, diffusion-time.

In order to further clarify that the water diffusion in CP is restricted, the radial signal changes for CP at T_{diff} = 37.7 and 97.7 ms can also be discussed using the q-space method.[22] The q-value is a spatial frequency determined according to the parameters of the applied MPG via the equation:

$$q = \frac{1}{2\pi}\gamma G\delta \qquad (4),$$

where γ is the gyromagnetic ratio, G is the magnitude of the MPG, and δ is the duration of the MPG lobe. The b-value can be written in terms of q in the following way

$$b = \gamma^2 G^2\delta^2(\Delta - \frac{\delta}{3}) = 4\pi^2 q^2(\Delta - \frac{\delta}{3}) \qquad (5),$$

where Δ is the time between the onsets of the MPG lobes, and $\Delta - \delta/3$ is the diffusion-time. The difference between the signal change patterns at T_{diff} = 37.7 and 97.7 ms in the radial direction for the CP is small when the signal is instead plotted against q-value (Fig. 4). This indicates that the majority of the difference between the radial signal decay curves when plotted against b-value (Fig. 3), is due to the different T_{diff}s. This is consistent with restricted diffusion dominant behavior for the CP.

The b-value-dependent signal changes in the axial direction were similar for both phantoms and T_{diff}s. Considering the facts that the volume fraction of the fast diffusion compartment (f_{fast}) was close to 1 and the corresponding diffusion coefficient (D_{fast}) was very large (more than 2.0×10^{-3} mm^2/s, Table 3), diffusion in the axial direction might have been close to that of free water.

Conclusion

In conclusion, the results of this study suggest that CP can be used as a restricted-diffusion dominant phantom, whereas Dy can be used as hindered-diffusion dominant phantom in a clinical setting. Both phantoms provided homogeneous DTI parameter maps. As it has a weaker dependence on diffusion-time and parameter estimates similar to those of brain white matter, Dy may be more suitable as a phantom for DTI QC.

Acknowledgments

The authors are grateful to Mr. Nobuhiro Nitta for assistance with the MRI experiments. The authors thank Dr. Ichio Aoki for the various discussions. This research was supported by a Grant-in-Aid for Scientific Research (KAKENHI, #15H04910) from the Japan Society for the Promotion of Science (JSPS), and by a grant from the Ministry of Education, Culture, Sports, Science and Technology (MEXT), Japanese Government.

Conflicts of Interest

The authors declare that they have no conflicts of interest.

References

1. Le Bihan D. The 'wet mind': water and functional neuroimaging. Phys Med Biol 2007; 52:R57–R90.
2. Shizukuishi T, Abe O, Aoki S. Diffusion tensor imaging analysis for psychiatric disorders. Magn Reson Med Sci 2013; 12:153–159.
3. Tachibana Y, Obata T, Yoshida M, et al. Analysis of normal-appearing white matter of multiple sclerosis by tensor-based two-compartment model of water diffusion. Eur Radiol 2015; 25:1701–1707.
4. Le Bihan D, Mangin JF, Poupon C, et al. Diffusion tensor imaging: concepts and applications. J Magn Reson Imaging 2001; 13:534–546.
5. Yanasak N, Allison J. Use of capillaries in the construction of an MRI phantom for the assessment of diffusion tensor imaging: demonstration of performance. Magn Reson Imaging 2006; 24:1349–1361.
6. Wang ZJ, Seo Y, Babcock E, et al. Assessment of diffusion tensor image quality across sites and vendors using the American College of Radiology head phantom. J Appl Clin Med Phys 2016; 17:442–451.
7. Kamagata K, Shimoji K, Hori M, et al. Intersite reliability of diffusion tensor imaging on two 3T scanners. Magn Reson Med Sci 2015; 14:227–233.
8. Melhem ER, Mori S, Mukundan G, Kraut MA, Pomper MG, van Zijl PC. Diffusion tensor MR imaging of the brain and white matter tractography. AJR Am J Roentgenol 2002; 178:3–16.
9. Sigmund EE, Song YQ. Multiple echo diffusion tensor acquisition technique. Magn Reson Imaging 2006; 24:7–18.
10. Freidlin RZ, Ozarslan E, Komlosh ME, et al. Parsimonious model selection for tissue segmentation and classification

applications: a study using simulated and experimental DTI data. IEEE Trans Med Imaging 2007; 26:1576–1584.
11. Leergaard TB, White NS, de Crespigny A, et al. Quantitative histological validation of diffusion MRI fiber orientation distributions in the rat brain. PLoS ONE 2010; 5:e8595.
12. Yanasak NE, Allison JD, Hu TC. An empirical characterization of the quality of DTI data and the efficacy of dyadic sorting. Magn Reson Imaging 2008; 26:122–132.
13. Oida T, Nagahara S, Kobayashi T. Acquisition parameters for diffusion tensor imaging to emphasize fractional anisotropy: phantom study. Magn Reson Med Sci 2011; 10:121–128.
14. Watanabe M, Aoki S, Masutani Y, et al. Flexible *ex vivo* phantoms for validation of diffusion tensor tractography on a clinical scanner. Radiat Med 2006; 24:605–609.
15. Fieremans E, De Deene Y, Delputte S, Ozdemir MS, Achten E, Lemahieu I. The design of anisotropic diffusion phantoms for the validation of diffusion weighted magnetic resonance imaging. Phys Med Biol 2008; 53:5405–5419.
16. Fieremans E, De Deene Y, Delputte S, et al. Simulation and experimental verification of the diffusion in an anisotropic fiber phantom. J Magn Reson 2008; 190:189–199.
17. Clark CA, Hedehus M, Moseley ME. Diffusion time dependence of the apparent diffusion tensor in healthy human brain and white matter disease. Magn Reson Med 2001; 45:1126–1129.
18. Porter DA, Heidemann RM. High resolution diffusion-weighted imaging using readout-segmented echo-planar imaging, parallel imaging and a two-dimensional navigator-based reacquisition. Magn Reson Med 2009; 62:468–475.
19. Niendorf T, Dijkhuizen RM, Norris DG, van Lookeren Campagne M, Nicolay K. Biexponential diffusion attenuation in various states of brain tissue: implications for diffusion-weighted imaging. Magn Reson Med 1996; 36:847–857.
20. Assaf Y, Freidlin RZ, Rohde GK, Basser PJ. New modeling and experimental framework to characterize hindered and restricted water diffusion in brain white matter. Magn Reson Med 2004; 52:965–978.
21. Clark CA, Le Bihan D. Water diffusion compartmentation and anisotropy at high b values in the human brain. Magn Reson Med 2000; 44:852–859.
22. Cohen Y, Assaf Y. High b-value q-space analyzed diffusion-weighted MRS and MRI in neuronal tissues - a technical review. NMR Biomed 2002; 15:516–542.